Jurnal Media Mesin, Vol. 23 No. 2
Printed-ISSN: 1411-4348
Online-ISSN: 2541-4577

COMPUTATIONAL FLUID DYNAMICS ANALYSIS BASED ON THE FLUID FLOW SEPARATION POINT ON THE UPPER SIDE OF THE NACA 0015 AIRFOIL WITH THE COEFFICIENT OF FRICTION

James Julian
Department of Mechanical Engineering, Faculty of Engineering
Universitas Pembangunan Nasional Veteran Jakarta
Email: zames@upnvj.ac.id

Waridho Iskandar
Department of Mechanical Engineering, Faculty of Engineering
Universitas Pembangunan Nasional Veteran Jakarta
Email: waridho.iskandar@upnvj.ac.id

Fitri Wahyuni
Department of Mechanical Engineering, Faculty of Engineering
Universitas Pembangunan Nasional Veteran Jakarta
Email: fitriwahyuni@upnvj.ac.id

Ferdyanto
Department of Electrical Engineering, Faculty of Engineering
Universitas Pembangunan Nasional Veteran Jakarta
Email: ferdyanto@upnvj.ac.id

ABSTRAK

Sebuah metode baru yang lebih praktis, efisien dan aplikatif diajukan untuk melacak posisi separasi aliran fluida di upper side NACA 0015. Metode yang diajukan adalah dengan metode kurva koefisien gesekan (C_f) pada permukaan atas airfoil. Pendekatan yang digunakan adalah pendekatan computational fluida dynamics (CFD). Persamaan pengatur yang digunakan adalah persamaan Reynolds Averaged Navier-Stokes (RANS). $k-\omega$ merupakan model turbulensi yang diimplementasikan pada penelitian ini. Penelitian dilakukan pada kategori bilangan Reynolds rendah. Bilangan Reynolds rendah berada pada rentang nilai 10^4 sampai dengan 3×10^5. Hasil yang diperoleh dari penelitian ini adalah C_f dapat memprediksi lokasi separasi aliran fluida dengan lebih praktis, efisien dan aplikatif jika dibandingkan dengan metode profil kecepatan aliran fluida. Separasi aliran mulai terbentuk pada α=8° pada posisi x/c=0.8. Lokasi separasi aliran fluida terus bergerak medekati leading edge jika α airfoil meningkat. Melaui kurva C_f, lokasi separasi aliran fluida adalah saat kurva C_f mengalami penuruan mendadak dan mendekati sumbu x. Jika digambarkan dalam bentuk profil kecepatan dan kontur kecepatan aliran fluida, maka akan terlihat penurunan vektor kecepatan yang ekstrim.
Kata kunci: airfoil, koefisien gesekan, komputasional, NACA 0015, pelacakan, titik separasi.

ABSTRACT

A new method that is more practical, efficient and applicable is proposed to track the position of fluid flow separation on the upper side of NACA 0015. The proposed method is the coefficient of friction curve (C_f) *method on the airfoil's upper side. The approach used is a computational fluid dynamics (CFD) approach. The governing equation used is the Reynolds Averaged Navier-Stokes (RANS) equation.* $k-\omega$ *is the turbulence model implemented in this study. The research is conducted on the low Reynolds number category. The low Reynolds number is in the range of values*

from 10^4 *to* 3×10^5. C_f *can predict the location of fluid flow separation more practically, efficiently, and applicable than the fluid flow velocity profile method. Flow separation begins to form at* $\alpha = 8°$ *at position x/c=0.8. The location of the fluid flow separation continues to move closer to the leading edge as the* α *airfoil increases. Through the* C_f *curve, the location of the fluid flow separation is when the* C_f *curve experiences a sudden decrease and approaches the x-axis. If the separation points are described in the form of velocity profiles and fluid flow velocity contours, it will form an extreme decrease.*
Keywords: *airfoil, coefficient of friction, computational, NACA 0015, separation point, track.*

1. INTRODUCTION

External fluid flow is an interesting topic for various research and development of fluid mechanics. In external fluid flow, various discussions can be explored. Among them is the ability of fluids to provide lift against an interacting body [1] [2]. One of the bodies that can generate lift when interacting with fluids is an airfoil [3] [4]. Because of their ability to generate lift, airfoils are used in aircraft, wind turbines, MAVs, and UAVs . The lift capacity of an airfoil is usually expressed in dimensionless units known as the lift coefficient (C_l) [5]. C_l data is usually presented in the curve of the change of C_l with the angle of attack (α). One of the characteristics of C_l is the stall condition. The stall condition is defined as a decrease in the value of C_l [6]. Stall conditions are caused by fluid flow separation on the upper side of the airfoil or wing. On the plane, this stall condition can cause the plane to experience a significant loss of lift and can cause the plane to experience a free fall. Various flow control devices can overcome fluid flow separation [7] [8]. Optimization of the use of flow control devices is very dependent on the location of the fluid flow separation point [9] [10]. Thus, a method is needed to quickly, practically, and precisely determine the separation point of fluid flow. One way that can be done is to detect the coefficient of friction (C_f) of the fluid flow against the surface of the airfoil.

Research on fluid flow separation has been carried out in many previous studies. Sudhakar and Kartikheyan conducted an experimental study related to the visualization of fluid flow separation on the upper side of NACA 4415. At α=18°, it is known that the fluid flow separation has been seen and covered 0.75 part of the upper side airfoil [11]. Dong et al. researched flow separation and transition on an airfoil at the low Reynolds number. The study was conducted experimentally and with CFD simulation. There are three variations of Reynolds number investigated, namely 200000, 300000 and 500000. Based on observations from the fluid flow velocity profile, at α =4° a laminar separation bubble has formed in the FX63-137 airfoil. The increase in α causes the location of the fluid flow separation to approach the leading edge of the airfoil. On the other hand, decreasing the Reynolds number causes the fluid flow separation location to approach the leading edge. Fluid flow separation is observed using a fluid flow velocity profile [12]. Another research is regarding the fluid flow separation point location on a symmetrical airfoil. The thicker the airfoil, the location of the flow separation will be closer to the leading edge. Meanwhile, an increase will make the fluid flow separation point on the upper side of the airfoil closer to the leading edge [13].

The above studies have summarized various things regarding the position of fluid flow separation at low Reynolds numbers. However, the method used to express the position of separation is not stated clearly and in-depth. Another study used the velocity profile method to find the position of the fluid flow separation. This method is quite complicated because it has to create many velocity profiles to determine the location of the fluid flow separation. Furthermore, this method will take much time and is inefficient because it requires at least two types of data, namely velocity contour data and velocity profile. Overall, a summary of what has been discussed in the studies above can be seen in Table 1. Thus, this study tries to provide an alternative way of tracking the location of fluid flow separation by determining the C_f value along the upper side of the airfoil. In this way, it is hoped that tracking fluid flow separation can be carried out quickly and precisely. This study aims to provide a new method for determining the location of fluid flow separation at a low Reynolds number. Low Reynolds number ranges from 10^4 to 3×10^5. The proposed method is to plot the C_f curve along the upper side of NACA 0015. Through the results of this study, it is hoped that determining the separation location will be more practical, efficient and applicable. In addition, this study also aims to complete various data related to fluid flow separation.

Table 1. Various studies about fluid flow separation.

Study	Visulization of fluid flow separation	Position of fuid flow separation in against α	Tracking fluid flow separation point using velocity profile	Tracking fluid flow separation point using C_f curve
Sudhakar and Karthikeyan, 2021 [11]	yes	no	no	no
Dong et al., 2019 [12]	yes	yes	yes	no
Frolov, 2016 [13]	no	yes	no	no
Zhang et al., 2015 [14]	yes	no	yes	no
Boutilier and Yarusevych, 2012 [15]	no	yes	yes	no
Current study	yes	yes	yes	yes

2. METHODOLOGY

This research uses numerical methods to simulate fluid flow, known as computational fluid dynamics (CFD). The CFD computation process is carried out by varying the α of the airfoil to collect aerodynamic data. In order to make the computation process more efficient, the α variation is done by changing the velocity vector of the fluid flow on the x-axis and y-axis, so there is no need to change the geometry and mesh to vary α of the airfoil. The data from this research are C_l, C_d, C_f and fluid flow contours. The data for C_l and C_d are grouped and sorted by α to get C_l and C_d curves for changes in α. Various aerodynamic information of NACA 0015 can be known through this curve, such as curve's trend, stall and $C_{l\,max}$. The C_l and C_d are validated by the previous study by Kekina and Suvanjumrat. The C_f curve of each α was proposed as a new method for tracking the location of fluid flow separation. It was used as the primary data in this study. The results of tracking the location of the fluid flow separation from the C_f curve are then compared with the commonly used method, namely by looking at the velocity profile of the fluid flow contour.

2.1 *NACA 0015*

The NACA 0015 airfoil is a type of airfoil created by the National Advisory Committee for Aeronautics (NACA) [16]. NACA 0015 is a symmetrical airfoil. The digit 0015 has its meaning; the number 0 in the first digit represents the maximum airfoil chamber. The second digit is the maximum position of the chamber. The airfoil's maximum thickness can be seen in the third and fourth digits, which is 15% of the chord length. The chord length of the airfoil used in this study is 1m. Overall, NACA 0015 can be seen in Figure 1.

Figure 1. NACA 0015 [17].

2.2 *Numerical method*

The numerical equation used in this study is the Reynolds Averaged Navier Stokes (RANS) equation. The constituent equations of the RANS equation are the continuity equation and the momentum equation. The RANS equation can be seen in equations 1 and 2 [18]. Equation 1 is the continuity equation of the fluid flow. Meanwhile, equation 2 is the momentum flow equation for fluid flow. The direction is analyzed and assumed to flow only in the direction of the x-axis.

$$\frac{\partial \rho}{\partial t} + \frac{\partial}{\partial x_i}\left(\rho u_i\right) = 0 \tag{1}$$

$$\frac{\partial}{\partial t}\left(\rho u_i\right) + \frac{\partial}{\partial x_i}\left(\rho u_i u_j\right) = \frac{\partial p}{\partial x_i} + \frac{\partial}{\partial x_j}\left[\mu\left(\frac{\partial u_i}{\partial x_j} + \frac{\partial u_j}{\partial x_i} - \frac{2}{3}\delta_{ij}\frac{\partial u_i}{\partial x_i}\right)\right] + \frac{\partial}{\partial x_i}\left(\rho\overline{u_i'u_j'}\right) \tag{2}$$

The turbulence model chosen in this study is standard $k-\omega$. The turbulence model was chosen because the model is suitable for simulating fluid flow with a low Reynolds number. The mathematical equations of the turbulence model can be seen in equations 3 and 4. Equation 3 is the transport equation for turbulent kinetic energy (k). Equation 4 is the equation for the specific dissipation rate (ω) [19].

$$\rho\frac{Dk}{Dt} = \tau_{ij}\frac{\partial\overline{u_i}}{\partial x_j} - \rho\beta^* f_{\beta^*} k\omega + \frac{\partial}{\partial x_j}\left[\left(\mu + \frac{\mu_t}{\sigma_k}\right)\frac{\partial k}{\partial x_j}\right] \tag{3}$$

$$\rho\frac{D\omega}{Dt} = \alpha\frac{\omega}{k}\tau_{ij}\frac{\partial\overline{u_i}}{\partial x_j} - \rho\beta f_{\beta}\omega^2 + \frac{\partial}{\partial x_j}\left[\left(\mu + \frac{\mu_t}{\sigma_\omega}\right)\frac{\partial\omega}{\partial x_j}\right] \tag{4}$$

2.3 *Domain, mesh and boundary condition*

The mesh made for this research is a structured mesh. The mesh element used is a mesh with a quadrilateral element shape. The main advantage of quadrilateral mesh is that it can be applied well to curved objects. So this mesh is very suitable for the NACA 0015 airfoil, which has a curvature on the upper and lower sides. Furthermore, the quadrilateral mesh can provide better quality with fewer elements than triangles mesh. The shape of the domain and the mesh in this study can be seen in Figure 2. The tail of the airfoil is placed right at the center of the circle of the domain [20]. This side of the domain is divided into two boundary conditions, namely velocity-inlet and pressure-outlet. Meanwhile, the boundary condition for the airfoil surface is the wall (no-slip). Overall, the boundary conditions in this study can be seen in Figure 2 (b). Furthermore, the boundary condition parameters can be seen in Table 2.

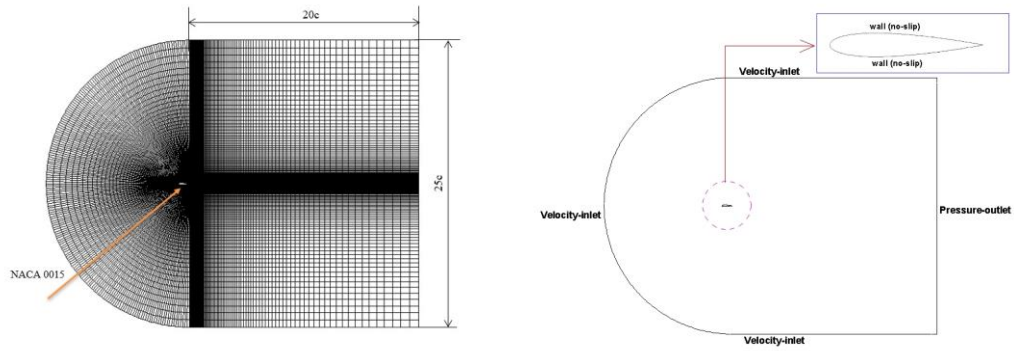

(a) Domain and mesh (b) Boundary condition

Figure 2. Details of model.

Table 2. Boundary condition parameters.

Properties	Values
Reynolds number	160000
Velocity-inlet	2.3371 m/s
Pressure-outlet	0 Pa
wall (no slip)	-

2.4 Mesh independence test

The mesh independence test in this paper is carried out using the Richardson extrapolation generalized by Roache. In this mesh independence test, there are several equations used. The first step is to determine the ratio of the grid variations with equation 5. The mesh independence test in this paper uses an order whose value is determined by equation 6. The Grid Convergence Index (GCI) is used to determine the error of the grid. There are two GCIs utilized in this paper. The first GCI is used to measure the error value between the fine and medium mesh, known as GCI_{fine}. The second GCI is the error value between the medium and coarse mesh known as GCI_{coarse}. The GCI_{fine} and GCI_{coarse} equations can be found in equations 7 and 8. There are two objectives in the mesh independence test. The first objective is to determine whether the mesh variation is within the convergence range; the equation used is equation 9. The second objective is to determine the number of meshes used for further computation; the selected mesh is the mesh that can give the smallest relative error to the parameter values. Parameter values can be determined by equation 10 [21].

$$r = \frac{h_2}{h_1} \tag{5}$$

$$\overline{p} = \frac{\ln\left(\frac{f_3 - f_2}{f_2 - f_1}\right)}{\ln(r)} \tag{6}$$

$$GCI_{fine} = \frac{F_s \,|\in|}{\left(r^{\overline{p}} - 1\right)} \tag{7}$$

$$GCI_{coarse} = \frac{F_s \,|\in| \, r^{\bar{p}}}{\left(r^{\bar{p}} - 1\right)} \tag{8}$$

$$\frac{GCI_{fine}}{GCI_{coarse} r^{\bar{p}}} \approx 1 \tag{9}$$

$$f\,\mathrm{r}_{h=0} = f_1 + \frac{(f_1 - f_2)}{\left(r^{\bar{p}} - 1\right)} \tag{10}$$

There are three types of mesh proposed for the mesh independence test. The highest number of elements is a fine mesh with 50000 elements. Meanwhile, the medium mesh is 25000 elements and the coarse mesh is 12500. The variation of the mesh can be seen in Figure 3.

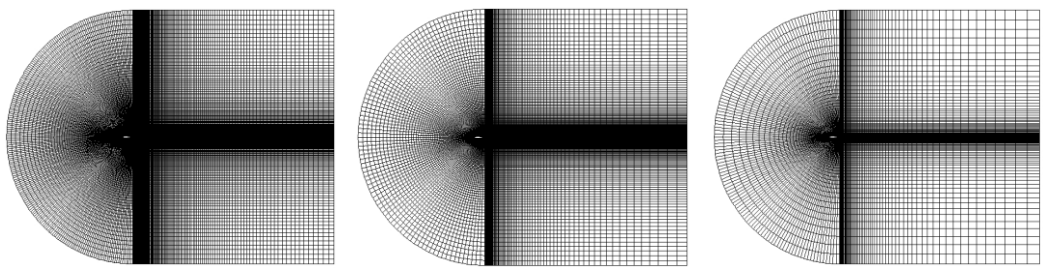

(a) fine (b) medium (c) coarse

Figure 3. Mesh variations.

The sample for the independent study mesh is the fluid flow velocity at X=0.2 and Y=0.2. The results of the independence test mesh can be said to be in the convergence range if $\frac{GCI_{fine}}{GCI_{coarse} r^{\bar{p}}} \approx 1$, as shown in table 3. The selected mesh is the mesh with the smallest number of errors. Based on table 3, it can be concluded that the mesh with 50000 elements is the most ideal for use in the next computational process.

Table 3. Mesh independence test results.

Mesh	Velocity	$\bar{p}$	r	GCI_{fine}	GCI_{coarse}	$f_{rh=0}$	$\frac{GCI_{fine}}{GCI_{coarse} r^{\bar{p}}}$	Error
Fine	3.27784	2.485575	2	0.180%	1.0160%	3.282565	1.006677	0.144%
Medium	3.2561							0.806%
Coarse	3.134344							4.515%

2.5 *Fluid flow separation*

Fluid flow separation is the phenomenon of the boundary layer separation from a body that interacts with the fluid. The boundary layer can be defined as a thin layer where the fluid surrounding the surface has a significant viscosity effect. Meanwhile, the fluid flow separation point can be interpreted as a point where the fluid flow separation begins. Boundary layer separation is caused by fluid particles losing energy to cross the object's surface while the fluid flows. The fluid flow in the flow separation will experience a back pressure

gradient so that if a velocity profile is made, it will show the direction of the velocity profile, which is reversed towards the upstream velocity [22]. Overall, the separated fluid flow and various related matters can be seen in Figure 4.

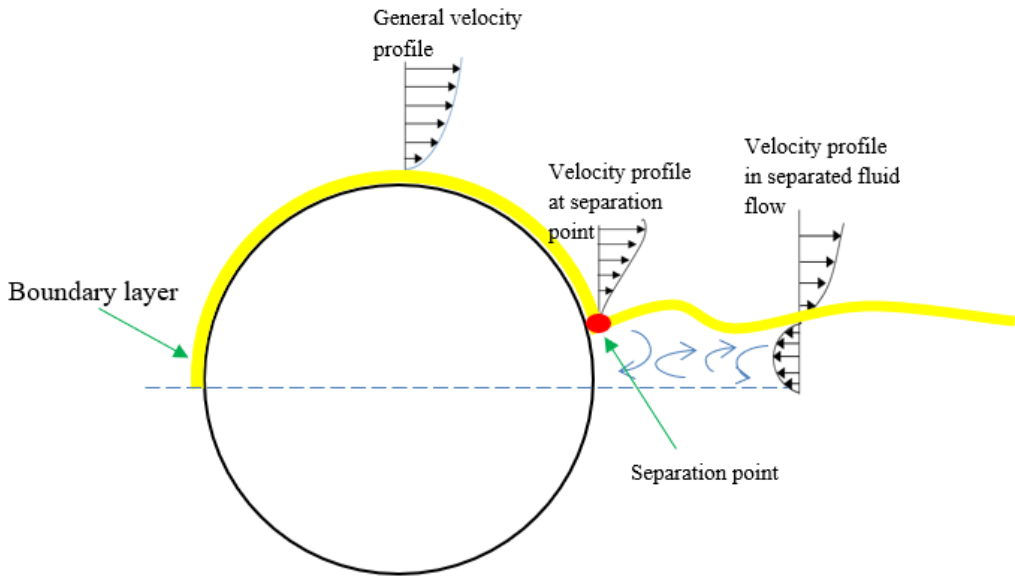

Figure 4. Fluid flow separation and related matters [22].

2.6 *Coefficient of friction*

The friction coefficient is a dimensionless value associated with the friction between the airfoil skin and the fluid. The mathematical equation C_f can be found in equation 11[23]. When a fluid passes through a surface, there will be a friction effect. The skin friction effect is caused by the viscosity of the fluid. This friction effect proves that no actual fluid is inviscid. Friction between the body's surface and the fluid predominantly occurs in the boundary layer. When the boundary layer is separated from the body's surface, the friction between the surface of the body and the fluid will decrease drastically [24]. In general, in the form of a C_f curve along the surface of the airfoil (x/c), as shown in Figure 5. The point of fluid flow separation can be detected when C_f approaches the value of 0 [25]. After passing the separation point, friction will occur again but at a number of the smaller ones. Friction on the airfoil surface when the fluid has undergone separation is caused by a change in the velocity profile towards the upstream velocity.

$$C_f = \frac{\tau_w}{0.5\rho U^2} \tag{11}$$

Where τ_w = *shear stress on airfoil surface*, ρ = *fluid density*, U = *Freestream-velocity* [23]

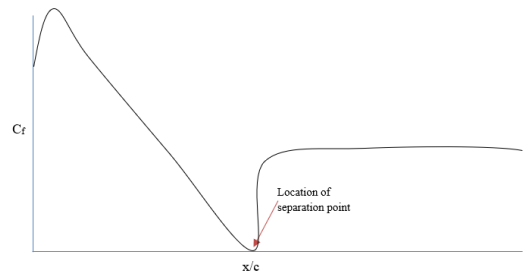

Figure 5. Fluid flow separation based on C_f [24].

3. RESULTS AND DISCUSSION

a) Validation

Before discussing the primary data of the CFD analysis, validation is needed to ensure that all models made can meet various actual fluid flow conditions. Validation was carried out with aerodynamic data such as C_l and C_d NACA 0015 at Reynolds number 160000. Comparative data for the validation process were experimental data from research conducted by Kekina and Suvanjumrat [26]. Figure 6 (a) shows the C_l data from the computational and experimental results. The C_l curve pattern from the experimental results and CFD generally shows a similar trend. At $\alpha \leq 10°$, the C_l curve shows conditions that tend to approach a linear form. At the $\alpha = 11°$, there was a sudden decrease in the value of C_l in the CFD and experimental data. This sudden decrease in C_l condition is known as a stall. This sudden decrease in C_l value was caused by the eruption of the laminar separation bubble on the upper side of the airfoil. Thus, the C_l curve shown in this study can be classified as a "drop curve". This stall condition also affects the value of C_d, where the experimental results and CFD show a very extreme increase, as shown in Figure 6(b). However, at $\alpha \leq 10°$, the C_d curve shows results that correspond to the experimental results and CFD.

In order to see the accuracy of CFD data specifically, it can be determined by looking at the error value. The error value is only calculated at $\alpha \leq 10°$. When $\alpha > 10°$, the error value is not calculated because the resulting aerodynamic data has become unstable and unpredictable. Overall the distribution of error values can be seen in table 4. The average error value for C_l is 4.900%, while the average error value for C_d is 30.51%. Thus, it can be concluded that the data obtained from the CFD results are quite valid and can be continued in the following discussion.

.

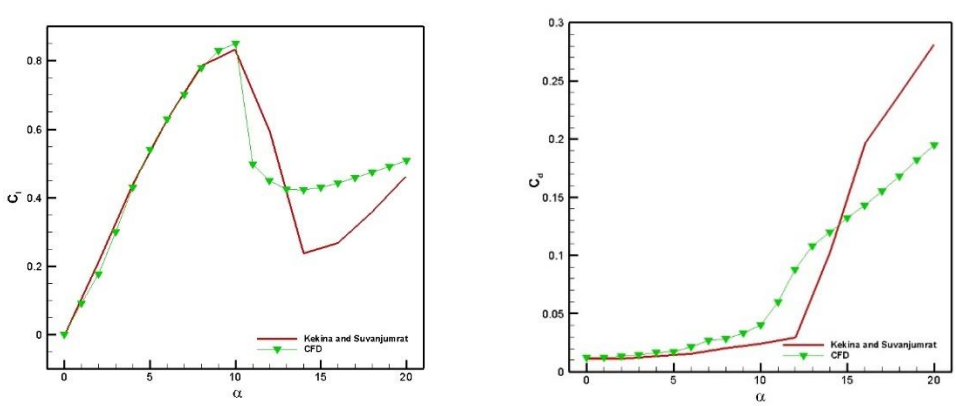

(a) C_l (b) C_d

Figure 6. Aerodynamic data.

Table 4. CFD data error value to experimental data.

α	Error value	
	C_l	C_d
0	2.500%	0.128%
1	15.587%	11.218%
2	17.521%	16.344%
3	8.285%	17.124%
4	2.184%	24.055%
5	1.218%	17.734%
6	0.414%	41.278%
7	0.794%	49.718%
8	0.485%	41.791%
9	2.634%	50.271%
10	2.274%	65.975%
Average	4.900%	30.51%

b) Analysis data

Figure 7 and 8 show the distribution curve of C_f on the upper side airfoil with $0^o \leq \alpha \leq 20°$. To simplify the observations, C_f is made in Figures 7 for $0^o \leq \alpha \leq 10^o$ and 8 for $11^o \leq \alpha \leq 20°$. Figure 7 shows that the fluid flow separation begins to form at $\alpha = 8^o$. The fluid flow separation position is at x/c=0.8. This separation condition then occurs at α =9° with the separation location at x/c=0.55 and α =10° with position x/c=0.29. Figure 8 shows that the fluid flow separation is formed in all α. The fluid flow separation point location will get closer to the leading edge as α increases.

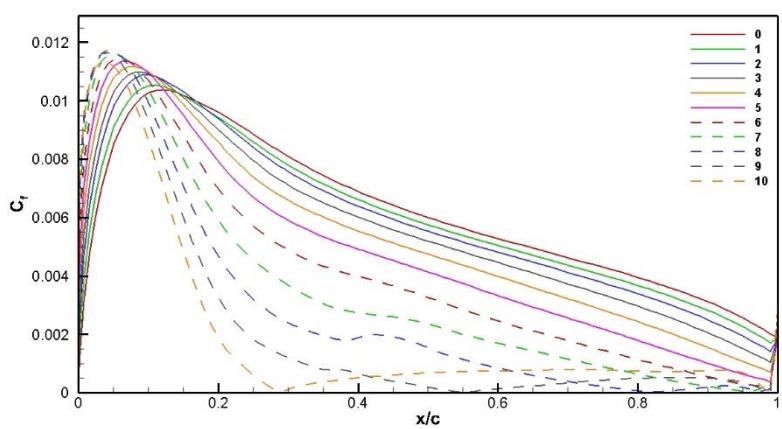

Figure 7. C_f on the upper side of airfoil at $0^o \leq \alpha \leq 10^o$.

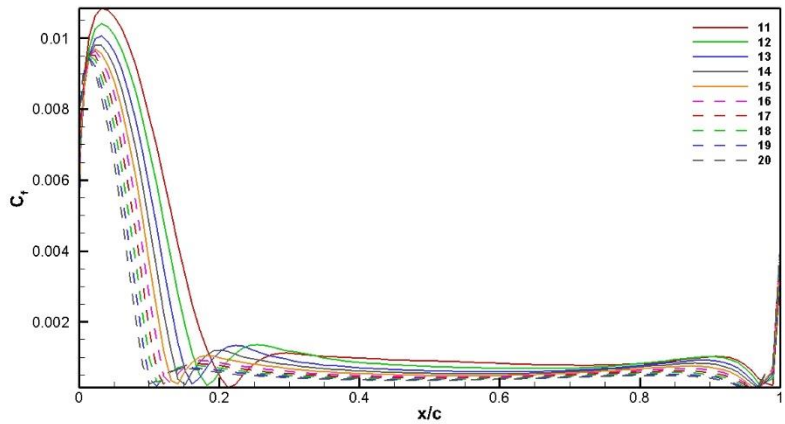

Figure 8. C_f on the upper side of airfoil at $11^o \leq \alpha \leq 20°$.

The fluid flow separation position curve at various α was made to compare with the results of the separation point position through C_f analysis. The curve is made based on the shape of the fluid velocity profile. Through Figure 9, it can be seen that the fluid flow separation begins to form at $\alpha = 8°$. The detection of fluid flow separation with velocity profile also shows that the location of the fluid flow separation is close to the leading edge of the airfoil. The location of the fluid flow separation can also be detected and shows results that correspond to the position of the fluid flow separation at the C_f curve.

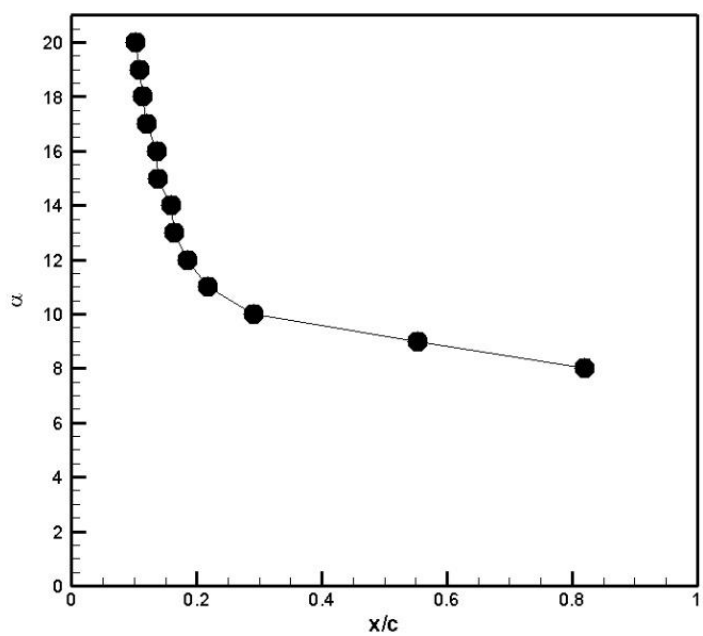

Figure 9. Location of separation points on some α.

Figure 10 shows the velocity profile on the upper side airfoil at α=11. There are three stages of the velocity profile displayed. The first fluid flow velocity profile is the fluid velocity profile under normal conditions without fluid flow separation. The velocity profile of the fluid decreases as the airfoil approaches the surface. However, the velocity profile near the airfoil surface can still be seen. The second velocity profile is the fluid velocity profile for flow at the separation point. Through this velocity profile, it can be seen that the fluid flow velocity profile decreases when approaching the airfoil surface. This drastic decrease in velocity profile is caused by the presence of a fluid flow separation point so that the velocity value is close to zero. The position of the separation point is at the position x/c=0.22. These results follow the results obtained in Figure 8. Meanwhile, the third velocity profile is the velocity profile of the separated fluid. This separated fluid flow profile is seen in the form of a velocity profile that is reversed or negative velocity.

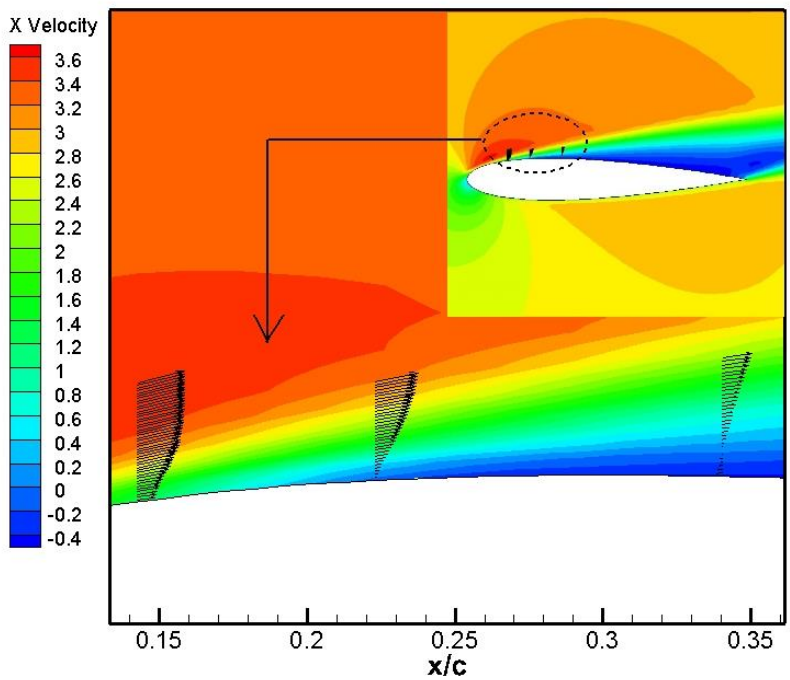

Figure 10. Velocity contour and profile on the upper side of airfoil.

4. CONCLUSION

Tracking fluid flow separation with the C_f curve method is proven to provide satisfactory results where the position of fluid flow separation is not much different when compared to the fluid flow velocity profile method. The C_f curve method is very efficient and easy to apply because it only requires C_f data without the need for fluid flow contours and fluid flow velocity profiles. Fluid flow separation begins to appear at α=8° at position x/c=0.8. If the α of the airfoil increases, the location of the fluid flow separation is getting closer to the leading edge. The separation on the C_f curve can be seen by the sudden decrease in the C_f value and the C_f value close to zero. The velocity profile method also shows the same results in terms of the initial separation and its position after the α increases. Overall, it can be concluded that the C_f curve method can track the fluid flow separation position more practically, applicable and efficiently compared to the fluid flow velocity profile method.

REFERENCES

[1] J. Julian, Harinaldi, Budiarso, C.-C. Wang, and M.-J. Chern, "Effect of plasma actuator in boundary layer on flat plate model with turbulent promoter," *Proceedings of the Institution of Mechanical Engineers, Part G: Journal of Aerospace Engineering*, vol. 232, no. 16, pp. 3001–3010, 2018, doi: 10.1177/0954410017727301.

[2] Harinaldi, Budiarso, J. Julian, and M. N. Rabbani, "The effect of plasma actuator on the depreciation of the aerodynamic drag on box model," in *AIP Conference Proceedings*, Jun. 2016, vol. 1737. doi: 10.1063/1.4949292.

[3] H. Harinaldi, B. Budiarso, F. Megawanto, R. Karim, N. Bunga, and J. Julian, "Flow Separation Delay on NACA 4415 Airfoil Using Plasma Actuator Effect," *International Review of Aerospace Engineering (IREASE)*, vol. 12, no. 4, 2019, doi: 10.15866/irease.v12i4.16219.

[4] E. A. Kosasih, R. F. Karim, and J. Julian, "Drag reduction by combination of flow control using inlet disturbance body and plasma actuator on cylinder model," *Journal of Mechanical Engineering and Sciences*, vol. 13, no. 1, pp. 4503–4511, Mar. 2019, doi: 10.15282/jmes.13.1.2019.12.0382.

[5] Budiarso, Harinaldi, Karim Riza Farrash, and Julian James, "Drag reduction due to recirculating bubble control using plasma actuator on a squareback model," *MATEC Web Conf.*, vol. 154, p. 1108, 2018, doi: 10.1051/matecconf/201815401108.

[6] Harinaldi, M. D. Kesuma, R. Irwansyah, J. Julian, and A. Satyadharma, "Flow control with multi-DBD plasma actuator on a delta wing," *Evergreen*, vol. 7, no. 4, pp. 602–608, 2020, doi: 10.5109/4150513.

[7] G.-C. Zha, W. Gao, and C. D. Paxton, "Jet Effects on Coflow Jet Airfoil Performance," *AIAA Journal*, vol. 45, no. 6, pp. 1222–1231, 2007, doi: 10.2514/1.23995.

[8] Harinaldi, A. S. Wibowo, J. Julian, and Budiarso, "The comparison of an analytical, experimental, and simulation approach for the average induced velocity of a dielectric barrier discharge (DBD)," *AIP Conference Proceedings*, vol. 2062, no. 1, p. 20027, 2019, doi: 10.1063/1.5086574.

[9] J. Julian, R. Karim, B. Budiarso, and H. Harinaldi, "Review: Flow Control on a Squareback Model," *International Review of Aerospace Engineering (IREASE)*, vol. 10, no. 4, 2017, doi: 10.15866/irease.v10i4.12636

[10] J. Julian, H. Harinaldi, B. Budiarso, R. Difitro, and P. Stefan, "The Effect of Plasma Actuator Placement on Drag Coefficient Reduction of Ahmed Body as an Aerodynamic Model," *International Journal of Technology*, vol. 7, no. 2, 2016, doi: 10.14716/ijtech.v7i2.2994

[11] S. Sudhakar and N. Karthikeyan, "Flow Separation Control on a NACA-4415 Airfoil at Low Reynolds Number," in *Lecture Notes in Mechanical Engineering*, 2021, pp. 323–334. doi: 10.1007/978-981-15-5183-3_35.

[12] H. Dong *et al.*, "Study on flow separation and transition of the airfoil in low Reynolds number," *Physics of Fluids*, vol. 31, no. 10, Oct. 2019, doi: 10.1063/1.5118736.

[13] V. A. Frolov, "Laminar separation point of flow on surface of symmetrical airfoil," in *AIP Conference Proceedings*, Oct. 2016, vol. 1770. doi: 10.1063/1.4963995.

[14] W. Zhang, W. Cheng, W. Gao, A. Qamar, and R. Samtaney, "Geometrical effects on the airfoil flow separation and transition," *Computers & Fluids*, vol. 116, pp. 60–73, 2015, doi: 10.1016/j.compfluid.2015.04.014.

[15] M. S. H. Boutilier and S. Yarusevych, "Parametric study of separation and transition characteristics over an airfoil at low Reynolds numbers," *Experiments in Fluids*, vol. 52, no. 6, pp. 1491–1506, Jun. 2012, doi: 10.1007/s00348-012-1270-z.

[16] P. D. Abd Aziz, A. K. R. Mohamad, F. Z. Hamidon, N. Mohamad, N. Salleh, and N. M. Yunus, "A simulation study on airfoils using VAWT design for low wind speed

application," in *2014 4th International Conference on Engineering Technology and Technopreneuship (ICE2T)*, 2014, pp. 105–109, doi: 10.1109/ICE2T.2014.7006228.

[17] K. A. Sunny, P. Kumar, S. Priscilla, and N. M. Kumar, "Computational analysis of three blade vertical axis wind turbine," *Progress in Industrial Ecology, An International Journal*, vol. 12, no. 1/2, p. 120, 2018, doi: 10.1504/pie.2018.10016967.

[18] H. Xiao and P. Cinnella, "Quantification of model uncertainty in RANS simulations: A review," *Progress in Aerospace Sciences*, vol. 108, pp. 1–31, 2019, doi:10.1016/j.paerosci.2018.10.001.

[19] S. M. A. Aftab, A. S. M. Rafie, N. A. Razak, and K. A. Ahmad, "Turbulence model selection for low reynolds number flows," *PLoS ONE*, vol. 11, no. 4, Apr. 2016, doi: 10.1371/journal.pone.0153755.

[20] F. C. Megawanto, Harinaldi, Budiarso, and J. Julian, "Numerical analysis of plasma actuator for drag reduction and lift enhancement on NACA 4415 airfoil," *AIP Conference Proceedings*, vol. 2001, no. 1, p. 50001, 2018, doi: 10.1063/1.5049992.

[21] P. J. Boache, "Perspective: A Method for Uniform Reporting of Grid Refinement Studies," , ASME. J. Fluids Eng, Vol. 116(3), pp405-413, 1994, doi: 10.1115/1.2910291

[22] M. Koklu and L. R. Owens, "Comparison of Sweeping Jet Actuators with Different Flow-Control Techniques for Flow-Separation Control," *AIAA Journal*, vol. 55, no. 3, pp. 848–860, 2017, doi: 10.2514/1.J055286.

[23] H. Takahashi, H. Iijima, M. Kurita, and S. Koga, "Evaluation of Skin Friction Drag Reduction in the Turbulent Boundary Layer Using Riblets," *Applied Sciences*, vol. 9, no. 23, 2019, doi: 10.3390/app9235199.

[24] Y. Zhang, Z. Zhou, K. Wang, and X. Li, "Aerodynamic characteristics of different airfoils under varied turbulence intensities at low Reynolds numbers," *Applied Sciences (Switzerland)*, vol. 10, no. 5, Mar. 2020, doi: 10.3390/app10051706.

[25] A. Choudhry, M. Arjomandi, and R. Kelso, "A study of long separation bubble on thick airfoils and its consequent effects," *International Journal of Heat and Fluid Flow*, vol. 52, pp. 84–96, Apr. 2015, doi: 10.1016/j.ijheatfluidflow.2014.12.001.

[26] P. Kekina and C. Suvanjumrat, "A Comparative Study on Turbulence Models for Simulation of Flow Past NACA 0015 Airfoil Using OpenFOAM.", In MATEC web of conferences, Vol. 95, p. 12005, doi: 10.1051/matecconf/20179512005